Applied Catalysis B: Environmental 94 (2010) 254–262

Contents lists available at ScienceDirect

Applied Catalysis B: Environmental

journal homepage: www.elsevier.com/locate/apcatb

Low temperature H_2-SCR over platinum catalysts supported on Ti-containing MCM-41

Landong Li [a], Peng Wu [a,b], Qing Yu [a], Guangjun Wu [a], Naijia Guan [a,*]

[a] Key Laboratory of Functional Polymer Materials, Ministry of Education, Institute of New catalytic Materials Science, Nankai University, Tianjin 300071, PR China
[b] China Shenhua Coal to Liquid and Chemical Beijing Research Institute, Beijing 100011, PR China

ARTICLE INFO

Article history:
Received 22 August 2009
Received in revised form 17 November 2009
Accepted 24 November 2009
Available online 3 December 2009

Keywords:
NO selective reduction
Hydrogen
Pt
Ti–MCM-41

ABSTRACT

A series of Ti-containing MCM-41 were prepared by isomorphously substitution, wet impregnation and mechanical mixing. Ti-containing MCM-41 materials, together with reference Si–MCM-41, were characterized by means of XRD, TEM and low temperature N_2 adsorption/desorption. The nature of Ti species on Ti-containing MCM-41 was analyzed by means of UV–vis and Raman spectroscopy. Pt catalysts supported on Si–MCM-41 and Ti-containing MCM-41 were studied for the selective catalytic reduction of NO by hydrogen in excess oxygen. Particular attention was paid to the promotion effect of different Ti species on the catalytic activity for H_2-SCR and the origin thereof. Pt/Ti–MCM-41 prepared by wet impregnation with the Ti/Si ratio of 0.6 exhibited the best activity and *ca.* 89% NO_x conversion as well as *ca.* 79% N_2 selectivity, could be achieved at 140 °C with a feed stream containing 1000 ppm NO, 5000 ppm H_2, 6.7% O_2 at a high GHSV of 80,000 h^{-1}. Moreover, Pt–Ti–MCM-41 exhibited good duration and good tolerance to co-existing 20 ppm SO_2 or 50 ppm CO, which demonstrated its potential for future applications.

1. Introduction

Nitrogen oxides are major air pollutants that greatly contribute to the formation of photochemical smog and acid rain [1]. Selective catalytic reduction of NO_x by ammonia (NH_3-SCR) is a well-known and widely investigated process for NO_x emissions control from stationary sources such as power plants and nitric acid plants [2]. Ammonia is industrially produced from hydrogen through Haber–Bosch process, so it is desirable to replace ammonia with less processed and less expensive nontoxic hydrogen. Hydrogen is very efficient reducing agent for NO_x reduction, however the NO–H_2 reaction over most catalysts is strongly inhibited by oxygen due to the competition between NO_x and O_2 in reacting with reductant hydrogen [3]. In recent studies, it has been found that the reduction of NO can be performed with H_2 even in excess oxygen at low temperatures. Therefore, H_2-SCR, which is regarded as possible alternative for NH_3-SCR, is receiving more and more attention.

Precious metal catalysts, *e.g.* Pt catalysts [4–11] and Pd catalysts [12–15], have been shown to be active for NO selective reduction by hydrogen at very low temperatures ($T < 200$ °C). Up to now, platinum seems to be the primary choice of active component for H_2-SCR reaction. Various supported platinum catalysts, *e.g.* Pt/SiO_2 [4], Pt/$La_{0.5}Ce_{0.5}MnO_3$ [5], Pt/TiO_2–ZrO_2 [6,7], Pt/Mg–Al–O [8], Pt/MFI [9], Na–Pt-ZSM-5 [10] and Pt/MgO–CeO_2 [11], have been applied in H_2-SCR reaction. The catalytic performance and reaction mechanism are investigated in details [16–18]. It is found that the types of support materials influence the oxidation states and dispersion of Pt, which are key issues controlling the activity in H_2-SCR reactions.

Mesoporous MCM-41, with regular arrangement of hexagonal channels and high surface area, has attracted much attention as a catalyst or a catalyst support. Especially, Pt/MCM-41 has been proven to be good catalyst for HC-SCR reaction [19–21]. In our previous work, we also found that Pt/MCM-41 exhibited much better activity in H_2-SCR reaction than Pt/silicate and Pt/SiO_2 [22]. However, the activity of Pt/MCM-41 is far from satisfying and further modification on the catalyst is highly desired.

In the present study, we will report a highly active Pt/Ti–MCM-41 catalyst for H_2-SCR reaction with feed stream containing 1000 ppm NO, 5000 ppm H_2, 6.7% O_2 at a high GHSV of 80,000 h^{-1}. The promotion effects of different Ti species on H_2-SCR activity are focused. For practical consideration, the durability of Pt/Ti–MCM-41 catalyst and its tolerance to co-existing SO_2 or CO are also investigated.

2. Experimental

2.1. Catalyst preparation

The Si–MCM-41 sample was synthesized according to the hydrothermal route reported in literature [23], with cetyltri-

* Corresponding author.
E-mail address: guannj@nankai.edu.cn (N. Guan).

0926-3373/$ – see front matter © 2009 Elsevier B.V. All rights reserved.
doi:10.1016/j.apcatb.2009.11.016

methylammonium bromide (CTAB) as template. Ti-containing MCM-41 materials were prepared by three different methods, *i.e.* isomorphously substitution, wet impregnation and mechanical mixing. For isomorphously substitution, a hydrothermal route similar to the synthesis of Si–MCM-41 was employed. Briefly, CTAB, tetraethyl orthosilicate (TEOS) and tetrabutyl orthotitanate (TBOT) were slowly added into distilled water in turn under stirring. The pH value of obtained gel was then adjusted to *ca.* 10.5. After stirred at 60 °C for 4 h, the gel (H_2O/CTAB/TEOS/TBOT = 8000/1/8/5) was transported into an autoclave for static crystallization at 110 °C for 12 h. The resulted solid was filtered, washed, dried at 80 °C for 12 h and then calcined in air at 500 °C for 4 h. The product was defined as [Ti]–MCM-41. For wet impregnation, 1 g MCM-41 support was suspended in 50 mL n-hexane and certain amount of TBOT was added. The mixture was refluxed for 24 h at the boiling point of n-hexane (68.7 °C) under the protection of nitrogen and then centrifuged. The obtained sample were dried at 80 °C and calcined in air at 500 °C. The final product was defined as Ti–MCM-41-*x*, where *x* indicating the Ti/Si ratio. For mechanical mixing, TiO_2 (Degussa P25) and Si–MCM-41 support with the Ti/Si ratio of 0.6 were well mixed and then calcined in air at 500 °C. The obtained product was defined as TiO_2–MCM-41.

Pt catalysts on different supports with Pt loading of *ca.* 1% were prepared by incipient wetness impregnation method, using potassium chloroplatinate as platinum precursor. The catalysts were dried at 80 °C for 12 h and then calcined in air at 500 °C for 3 h.

2.2. Catalyst characterization

Powder X-ray diffraction (XRD) measurements were performed on the samples using a Rigaku D/max 2500 diffractometer, equipped with a graphite monochromator and using Cu Kα radiation.

The textural properties of samples were analyzed by low temperature N_2 adsorption/desorption using a Quantachrome NOVA-1200 gas absorption analyzer and the specific surface areas were calculated using the BET equation.

Transmission electron microscopy (TEM) images of samples were acquired on a Tecnai G^2 2010 S-TWIN transmission electron microscope at an accelerate voltage of 200 kV.

The dispersion of platinum in different catalysts was determined by H_2 pulse adsorption on a chemisorption analyzer (Chemisorb 2720, Micromeritics). In a typical experiment, *ca.* 100 mg sample in the quartz reactor was pre-oxidized in O_2/He at 400 °C for 1 h to ensure removal of hydrocarbons on the surface and then cooled to room temperature in flowing He. Subsequently, the sample was heated in 5%H_2/Ar to 350 °C, reduced in 5%H_2/Ar at 350 °C for 1 h and then treated in He at 350 °C until no hydrogen desorption can be observed. The possible hydrogen spillover is believed to be eliminated. After cooling down to room temperature in flowing He, pulses of H_2 were injected to the reactor every one minute until no further changes in intensity of outlet H_2 (*ca.* 20 min). The dispersion of platinum was calculated assuming the equimolar adsorption of H on platinum.

The nature of Ti species on Ti-containing MCM-41 was analyzed by UV–vis and Raman spectroscopy. Diffuse reflectance UV–vis spectra were recorded in the air against $BaSO_4$ in the region of 200–700 nm on a HP8453 UV–vis spectrophotometer. Raman spectroscopy was carried out with a Renishaw InVia Raman spectrometer and spectra were obtained with the green line of an Ar-ion laser (514.53 nm) in micro-Raman configuration.

X-ray photoelectron spectra (XPS) were recorded on a Kratos Axis Ultra DLD spectrometer with a monochromated Al Kα X-ray source ($h\nu$ = 1486.6 eV), hybrid (magnetic/electrostatic) optics and a multi-channel plate and delay line detector (DLD). All spectra were recorded using an aperture slot of 300 μm × 700 μm, survey spectra were recorded with a pass energy of 160 eV and high-resolution spectra with a pass energy of 40 eV. Accurate binding energies (±0.1 eV) were determined with respect to the position of the adventitious C 1s peak at 284.8 eV. Prior to XPS, the samples were calcined in O_2/He (6.7% O_2, 100 mL min^{-1}) for 1 h at 400 °C.

2.3. Catalytic testing

The selective catalytic reduction of NO by hydrogen at atmospheric pressure was carried out in a fixed-bed flow microreactor. The typical reactant gas composition was NO (1000 ppm), H_2 (5000 ppm), O_2 (6.7%), and the balance He. The total flow of the inlet gas was set at 200 mL min^{-1}. A sample weight of 100 mg was employed, corresponding to the gas hourly space velocity (GHSV, based on catalyst volume) of 80,000 h^{-1}. Prior to testing, the samples were calcined in O_2/He (6.7% O_2, 100 mL min^{-1}) for 1 h at 400 °C. The products were analyzed on-line using a gas chromatograph (HP 6820 series, for N_2 and N_2O analysis) and a chemiluminescence NO_x analyzer (Ecotech EC 9841, for NO and NO_2 analysis). The nitrogen balance is calculated for each step using the following equation, where NO_x is the sum of NO and NO_2: $[NO_x]_{inlet} = [NO_x]_{outlet} + 2[N_2O]_{outlet} + 2[N_2]_{outlet}$. This N-balance was found to be >95% for all experiments. The NO_x conversion is calculated as $X_{NO_x} = ([NO_x]_{inlet} - [NO_x]_{outlet})/[NO_x]_{inlet}$. The N_2 selectivity is calculated as $S_{N_2} = 2[N_2]/([NO_x]_{inlet} - [NO_x]_{outlet})$ while the N_2O selectivity is calculated as $S_{N_2O} = 2[N_2O]/([NO_x]_{inlet} - [NO_x]_{outlet})$.

3. Results and discussion

3.1. Characterization of Ti-containing MCM-41

The XRD patterns of Si–MCM-41 and Ti-containing MCM-41 samples are shown in Fig. 1. For Si–MCM-41, an intense (1 0 0) diffraction peak ($2\theta = 2.1°$), together weak (1 1 0) diffraction peak ($2\theta = 3.6°$) and weak (2 0 0) diffraction peak ($2\theta = 4.2°$), is clearly observed, corresponding to the characteristic MCM-41 structure [23]. For Ti–MCM-41 and TiO_2–MCM-41, similar peaks are also observed, indicating that the hexagonally order structure are well

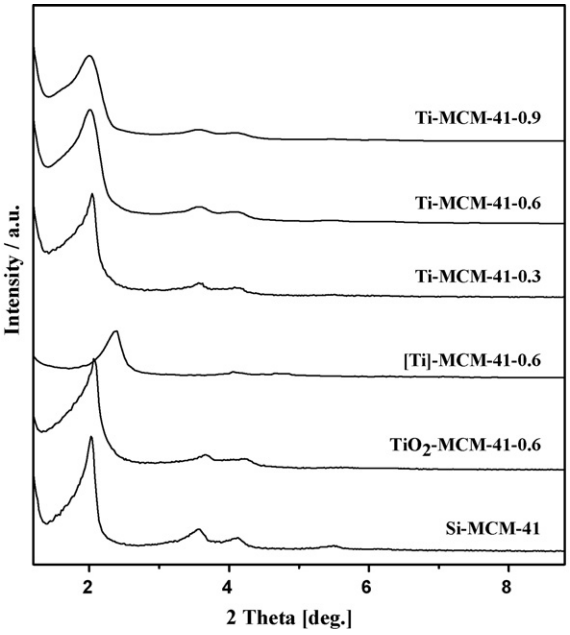

Fig. 1. XRD patterns of Si–MCM-41 and Ti-containing MCM-41 prepared by different methods.

Table 1
Textural properties of Ti-containing MCM-41 and Si–MCM-41 samples.

Sample	S_{BET} (m^2/g)	Pore volume (cm^3/g)	Pore diameter (nm)	Wall thickness (nm)[a]
Si–MCM-41	1176	0.96	3.33	1.12
Ti–MCM-41-0.3	868	0.63	3.28	1.67
Ti–MCM-41-0.6	857	0.61	3.20	1.79
Ti–MCM-41-0.9	840	0.59	3.14	1.92
[Ti]–MCM-41-0.6	596	0.56	3.08	1.20
TiO_2–MCM-41-0.6	759	0.49	3.28	1.19

[a] Calculated by subtracting the pore diameter from the unit cell parameter.

preserved after the introduction of Ti species by wet impregnation or mechanical mixing. While for [Ti]–MCM-41, due to the isomorphously substitution of framework Si^{4+} by Ti^{4+} with much larger radius, the hexagonal pores become smaller and the order pores are partially destroyed. As reflected in the XRD pattern, the intense (1 0 0) diffraction peak is observed at $2\theta = 2.4^\circ$ and the peak intensity decreases to some extent compared to Si–MCM-41.

The textural properties of Ti-containing MCM-41 and Si–MCM-41 samples are listed in Table 1. It is seen that the introduction of Ti species to Si–MCM-41 results in general decreases in the specific

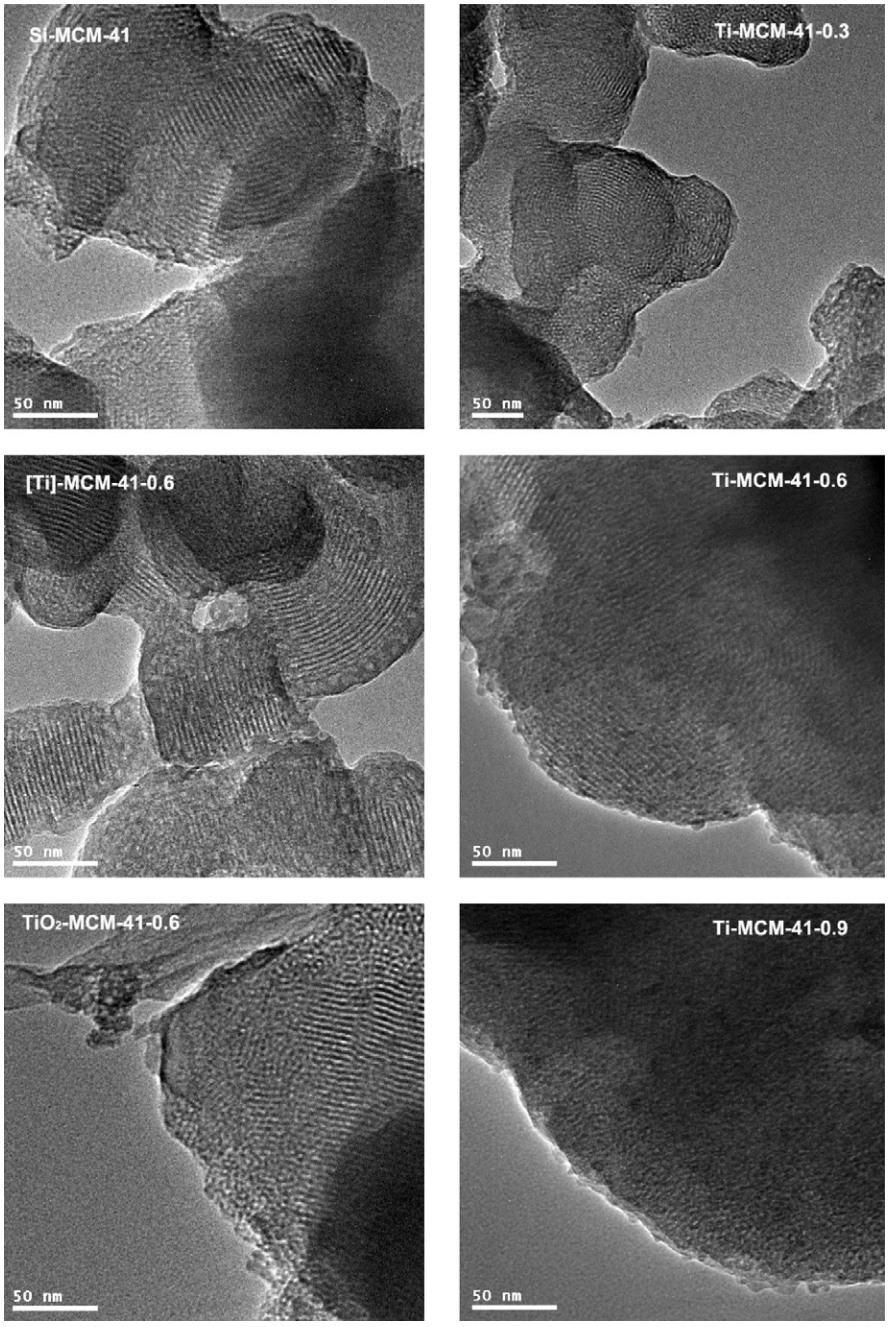

Fig. 2. TEM images of Si–MCM-41 and Ti-containing MCM-41 prepared by different methods.

surface areas and the pore volumes. However, mesopores of >3 nm are still obtained on Ti-containing samples, suggesting that the pores are not heavily blocked by the existence of Ti species. Moreover, the pore wall of Si–MCM-41 becomes thicker and pore size becomes smaller after the introduction of Ti species by wet impregnation. The changes become more obvious with higher Ti loadings. It is thus proposed that the impregnated Ti species mainly exist on the surface of Si–MCM-41 mesopores.

Fig. 2 shows the representative TEM images of Si–MCM-41 and Ti-containing MCM-41 samples. The worm-like morphology consisting of mesoporous is clearly observed for Si–MCM-41 sample. Similar morphology is also obtained on [Ti]–MCM-41-0.6 sample. It is proposed that most Ti atoms substitute Si atoms in the framework of MCM-41 structure and these Ti atoms cannot be distinguished in TEM images. For TiO_2–MCM-41-0.6 sample, irregular crystals are observed besides the MCM-41 morphology, indicating the existence of both TiO_2 and MCM-41 after mechanical mixing. While for Ti–MCM-41-0.6, uniform separated nanoparticles of *ca.* 2 nm are embedded in the mesoporous structure of MCM-41. At lower Ti/Si ratio of 0.3 (Ti–MCM-41-0.3), no nanoparticles can be distinguished while at higher Ti/Si ratio of 0.9 (Ti–MCM-41-0.9), nanoparticles with much larger size are observed. It is deduced that nanoparticles (probably TiO_2) embedded in mesoporous structure of MCM-41 can be obtained after wet impregnation at high Ti/Si ratios and the sizes of nanoparticles are dependent on the Ti/Si ratios, *i.e.* Ti loadings in Ti–MCM-41.

The nature of surface Ti species on Ti-containing MCM-41 is analyzed by means of Raman spectra. As displayed in Fig. 3, strong bands at 145, 400, 520 and 640 cm^{-1} are observed for TiO_2–MCM-41-0.6, corresponding to the Raman-active modes of anatase with the symmetries of E_g, B_{1g}, A_{1g}, and E_g, respectively [24]. In contrast, no Raman-active bands are observed on [Ti]–MCM-41-0.6, indicating the absence of surface anatase phase. For Ti–MCM-41, no surface anatase phase is detected at low Ti/Si ratio of 0.3 while surface anatase is detected in Raman spectra at high Ti/Si ratio of 0.6 and 0.9.

UV–vis spectroscopy is a powerful method for the characterization of Ti species and the UV–vis spectra of Ti-containing MCM-41 samples are shown in Fig. 4. A strong absorbance band at *ca.* 210 nm and a shoulder band at *ca.* 260 nm are observed on [Ti]–MCM-41. The band at *ca.* 210 nm is attributed to ligand-to-metal charge transfer associated with isolated Ti atoms in tetrahedral coordination while the band at *ca.* 260 nm is attributed to isolated Ti atoms in pentahedral or octahedral coordination [25,26]. Therefore, it is believed most Ti atoms should substitute Si in the framework or surface in [Ti]–MCM-41 with the formation of Ti–O–Si–O–Ti band. For TiO_2–MCM-41, adsorption bands at *ca.* 220, 260 and 320 nm are clearly observed in the UV–vis spectra. The band at *ca.* 320 nm is typical for ligand-to-metal charge transfer occurring on bulk titania [27], indicating the existence of bulk TiO_2 in TiO_2–MCM-41. The band at *ca.* 220 is attributed to isolated Ti atoms with distorted tetrahedral environment [28]. Obviously, Ti species exist in the form of both isolated Ti atoms and bulk TiO_2 through mechanical mixing and subsequent calcination. For Ti–MCM-41, isolated Ti atoms are exclusive Ti species at low Ti loading (Ti/Si = 0.3), while bulk TiO_2 species appear at high Ti loadings (Ti/Si = 0.9). It is seen from the TEM images that Ti species exist as nanoparticles embedded in the mesoporous structure of Ti–MCM-41 with different sizes at different Ti/Si ratios. From Raman and UV–vis analysis, the Ti species are recognized as bulk anatase TiO_2 at Ti/Si ratio of 0.9 while they are recognized as highly dispersed anatase nanoparticles at Ti/Si ratio of 0.6.

Based on all above characterization results, we can see that different Ti species can be introduced to MCM-41 by different methods with the mesoporous structure well preserved. Through isomorphously substitution, Ti species may go into the framework of MCM-41 and mainly exist as isolated Ti atoms in tetrahedral coordination. Through mechanical mixing and subsequent calcination, Ti species may exist in both isolated Ti atoms (in distorted tetrahedral coordination) and bulk anatase phase. While for Ti–MCM-41 prepared by wet impregnation, the existence form of Ti species is dependent on Ti loadings. At low Ti loading (Ti/Si = 0.3), Ti species mainly exist in the form isolated Ti atoms in distorted tetrahedral coordination. At high Ti loadings (Ti/Si = 0.9), Ti species exist in the form of both isolated atoms with distorted tetrahedral environment and bulk TiO_2. At Ti/Si ratio of 0.6, Ti species existence in the form of isolated Ti atoms and highly dispersed anatase nanoparticles embedded in MCM-41 mesoporous structure.

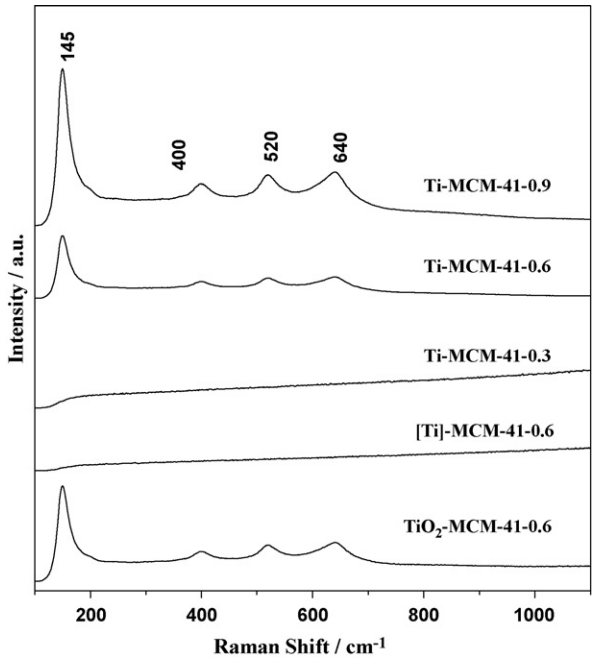

Fig. 3. Raman spectra of Ti-containing MCM-41 prepared by different methods.

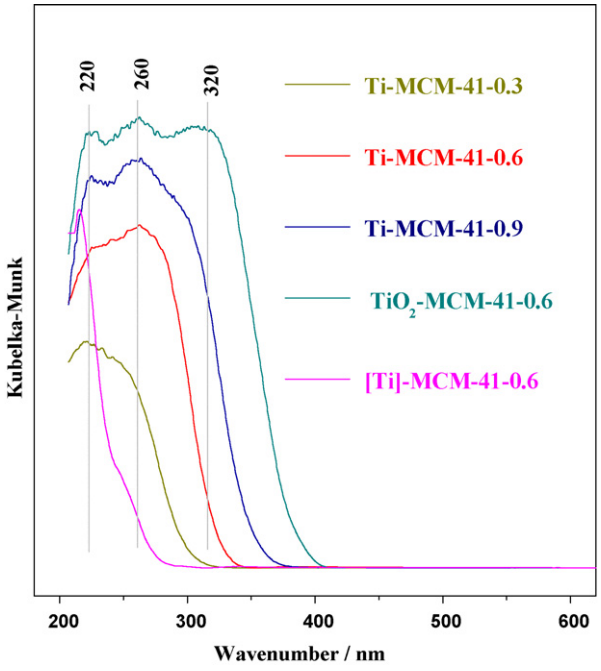

Fig. 4. UV–vis spectra of Ti-containing MCM-41 prepared by different methods.

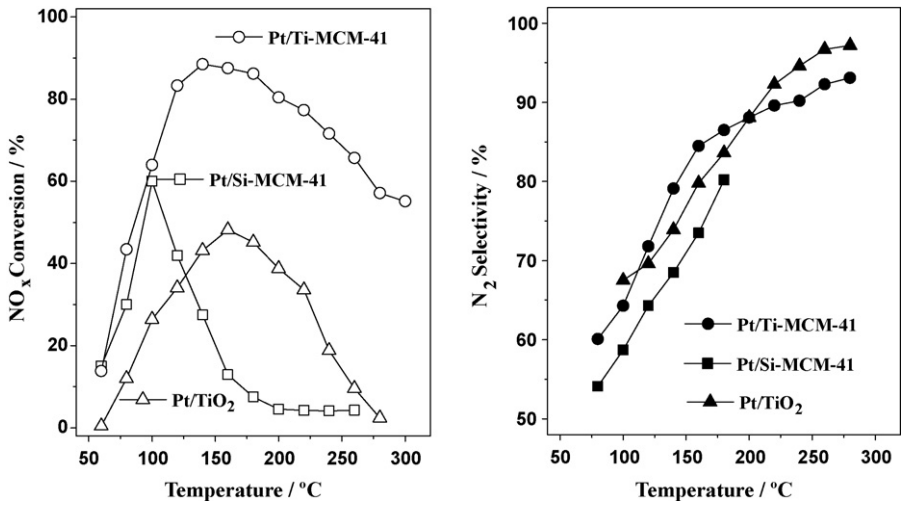

Fig. 5. NO_x conversion and N_2 selectivity on Pt/Ti–MCM-41 (Ti/Si = 0.6), Pt/Si–MCM-41 and Pt/TiO_2. *Reaction conditions*: NO = 1000 ppm, H_2 = 5000 ppm, O_2 = 6.7%, He balance, GHSV = 80,000 h^{-1}.

3.2. Catalytic performance of different Pt catalysts in H_2-SCR reaction

The temperature dependence of steady-state H_2-SCR reaction (reaction at constant temperature for 1 h) over different Pt catalysts is shown in Fig. 5. It is seen that the support materials have great effects on the activity of Pt catalysts. A maximal NO_x conversion of *ca.* 48% is obtained at 160 °C on Pt/TiO_2 while a maximal NO_x conversion of *ca.* 60% is obtained at 100 °C on Pt/Si–MCM-41. After the introduction of Ti species to Si–MCM-41 support by wet impregnation (Ti/Si = 0.6), the activity of Pt catalyst is greatly promoted and a maximal NO_x conversion of *ca.* 89% is obtained at 140 °C. In our experiments, two types of N-containing products are detected: N_2 as the target ideal product and N_2O as undesired by-product. Fortunately, Pt/TiO_2, Pt/Si–MCM-41 and Pt/Ti–MCM-41 all exhibit relative high N_2 selectivity and the N_2 selectivity over these catalysts increases with increasing reaction temperature, as seen in Fig. 5. For Pt/Ti–MCM-41, high N_2 selectivity of *ca.* 79% is achieved at 140 °C when maximal NO_x conversion is obtained. It is worthy mentioning that the catalytic performance (activity and selectivity) of Pt/Ti–MCM-41 for H_2-SCR reaction is comparable with most supported Pt catalysts reported elsewhere to our knowledge. For a direct comparison, the catalytic performance of supported Pt catalysts for H_2-SCR reaction under comparable conditions is summarized in Table 2.

We further investigate the H_2-SCR activity of Pt catalysts supported on Ti-containing MCM-41 prepared by different methods. As seen in Fig. 6, the best activity is achieved on Pt/Ti–MCM-41, followed by Pt/TiO_2–MCM-41 and then Pt/[Ti]–MCM-41 at identical Ti/Si ratio of 0.6. The promotion effect of Ti on Pt/Si–MCM-41 is evident when Ti-containing MCM-41 support is prepared by wet impregnation or mechanical mixing. In contrast, no obvious promotion effect is observed when the support is prepared by isomorphously substitution. Besides the preparation methods of Ti-containing MCM-41 support, the Ti/Si ratios are also very important for the promotion effect. The best activity is achieved on Pt/Ti–MCM-41-0.6, followed by Pt/Ti–MCM-41-0.9 and then Pt/Ti–MCM-41-0.3. The reason for the activity order will be discussed in the following section.

3.3. The promotion effect of Ti species in Pt/Ti–MCM-41

It is seen from above catalytic results that the introduction of Ti species may show great promotion effect on H_2-SCR over Pt/MCM-41 catalyst and the promotion effect is very much related to preparation methods for Ti-containing MCM-41 and the resulted Ti/Si ratios. Characterization results confirm that different Ti species are formed through different methods of Ti-containing MCM-41 or at different Ti/Si ratios. It is thus proposed that different Ti species show different effect on H_2-SCR over Pt/MCM-41, probably by forming different Pt–Ti interaction. Highly dispersed anatase nanoparticles embedded in the mesoporous structure of MCM-41 show the best promotion effect on Pt catalysts supported on Ti-containing MCM-41.

Fig. 7 shows the XPS of Pt 4f region of different Pt catalysts. For Pt/TiO_2, $Pt^{II}O$ (binding energy at 72.4 eV and 75.7 eV) and $Pt^{IV}O_2$ (binding energy at 73.7 eV and 77.1 eV) [29,30] are observed on

Table 2
Comparison of different Pt catalysts for H_2-SCR reaction.

Catalyst	Pt loading	Reaction conditions	NO conversion	N_2 selectivity	Reaction temperature	Reference
Pt/$La_{0.5}Ce_{0.5}MnO_3$	**0.1%**	NO = 0.25%, H_2 = 1%, O_2 = 5%, GHSV = 80,000 h^{-1}	74%	75%	140 °C	[5]
Pt/Al_2O_3	1%	NO = 800 ppm, H_2 = 2800 ppm, O_2 = 10%, W/F = 0.24 s g cm^{-3}	92%	40%	80 °C	[6]
Pt/TiO_2–ZrO_2	1%	NO = 800 ppm, H_2 = 2800 ppm, O_2 = 10%, W/F = 0.24 s g cm^{-3}	89%	53%	90 °C	[6]
Pt/Mg–Al–O	1%	NO = 800 ppm, H_2 = 2800 ppm, O_2 = 10%, W/F = 0.24 s g cm^{-3}	83%	53%	70 °C	[8]
Na–Pt–ZSM-5	1%	NO = 800 ppm, H_2 = 2800 ppm, O_2 = 10%, W/F = 0.24 s g cm^{-3}	95%	32%	70 °C	[10]
Pt/ZSM-5	0.8%	NO = 1000 ppm, H_2 = 5000 ppm, O_2 = 6.7%, GHSV = 78,000 h^{-1}	96%	70%	100 °C	[9]
Pt/MgO–CeO_2	**0.1%**	NO = 0.25%, H_2= 1%, O_2 = 5%, GHSV = 80,000 h^{-1}	95%	75%	150 °C	[11][a]
Pt/ZSM-5[b]	1%	NO = 1000 ppm, H_2 = 5000 ppm, O_2 = 6.7%, GHSV = 80,000 h^{-1}	84%	62%	120 °C	This work
Pt/Si–MCM-41	1%	NO = 1000 ppm, H_2 = 5000 ppm, O_2 = 6.7%, GHSV = 80,000 h^{-1}	60%	59%	100 °C	This work
Pt/Ti–MCM-41	1%	NO = 1000 ppm, H_2 = 5000 ppm, O_2 = 6.7%, GHSV = 80,000 h^{-1}	89%	79%	140 °C	This work

The bold values are required by one reviewer to emphasize the low Pt loadings in these catalysts.
[a] High activity and selectivity are achieved even in the presence of 5% H_2O and 10% CO_2.
[b] Prepared by impregnation H-ZSM-5 (Si/Al = 25) with $Pt(NH_3)_4Cl_2$ aqueous solution.

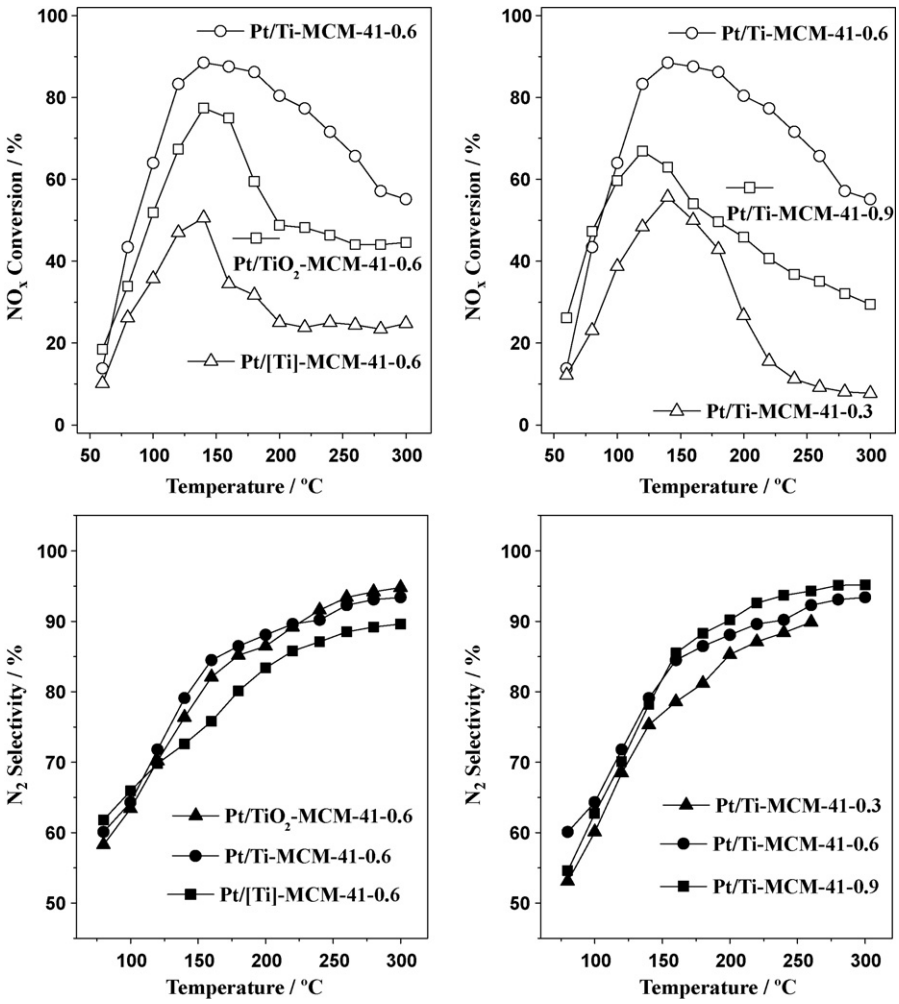

Fig. 6. NO_x conversion and N_2 selectivity on Pt supported on different Ti-containing MCM-41 samples. *Reaction conditions*: NO = 1000 ppm, H_2 = 5000 ppm, O_2 = 6.7%, He balance, GHSV = 80,000 h^{-1}.

TiO_2 support. For Pt/Si–MCM-41, metallic Pt^0 (binding energy at 70.7 eV and 74.1 eV) [31] and $Pt^{II}O$ (binding energy at 72.4 eV and 75.7 eV) are observed on Si–MCM-41 support. Obviously, the support materials play a decisive role on the existence status of Pt species. The introduction of Ti species to Si–MCM-41 results in great changes in the existence status of Pt species. For Pt/[Ti]–MCM-41, Pt^0 and $Pt^{II}O$ are observed similar to that observed on Pt/Si–MCM-41 while a higher proportion of Pt^0 is obtained. With the introduction of Ti species, Pt–Ti electron-interaction may form and electrons are donated from Ti species to Pt species. As a result, the Pt species may be reduced by the donated electrons to some extent [32]. For Pt/TiO_2–MCM-41, Pt^0, $Pt^{II}O$ and $Pt^{IV}O_2$ are observed on TiO_2–MCM-41 support. Based on the properties of TiO_2–MCM-41, we propose that some Pt species ($Pt^{II}O$ and $Pt^{IV}O_2$) are located on bulk TiO_2 and some (Pt^0 and $Pt^{II}O$) are located on MCM-41 mesoporous structure. For Pt/Ti–MCM-41, the existence status of Pt is quite complicated and dependent on Ti/Si ratios. Pt^0 and $Pt^{II}O$ are observed on Ti–MCM-41 at Ti/Si ratio of 0.3 or 0.6, while $Pt^{IV}O_2$ appears at higher Ti/Si ratio of 0.9. A reasonable explanation is that bulk TiO_2 is formed at Ti/Si ratio of 0.9 and some Ti species are located on bulk TiO_2 as $Pt^{II}O$ and $Pt^{IV}O_2$. The detailed valence distribution of Pt species in different Pt catalysts is summarized in Table 3. Integrated with the characterization results on Ti-containing MCM-41, it is concluded that the introduction of isolated Ti atoms or highly dispersed anatase nanoparticles leads to the partially reduction of $Pt^{II}O$ to Pt^0 by the electrons donated from Ti species to Pt species while the introduction of bulk TiO_2 leads to the appearance of $Pt^{IV}O_2$ and $Pt^{II}O$ located on bulk TiO_2. As is known, Pt^0 species act as the adsorption sites for reactant and as the active sites for surface reaction during SCR process [33,34]. From this point of view, the reduction of $Pt^{II}O$ to Pt^0 originated from the introduction of Ti species undoubtedly favors the progress of H_2-SCR reaction.

Besides the changes in the valence distribution of Pt species, the introduction of Ti species to Si–MCM-41 support also results in the changes in Pt dispersion. As displayed in Table 3, the Pt dispersion is improved in varying degrees after the introduction of Ti species by different methods. Typically, the highest Pt dispersion of 74.3% is obtained on Pt/Ti–MCM-41-0.6, in great contrast to the 33.4% on Pt/Si–MCM-41. The improvement in Pt dispersion may also be explained from the formation of Pt–Ti interaction. With the introduction of Ti species, the Pt species on supports may not only interact with the mesoporous structure of MCM-41 but also interact with the introduced Ti species. In such a manner, Pt nanoparticles are greatly stabilized and the aggregation or sintering of Pt species is greatly prevented. It is well known that the reduction of NO on Pt is sensitive to Pt structure. As for H_2-SCR, the key step of NO dissociation (NO → N + O) is energy preferred on stepped {2 1 1} surface than that on flat {1 1 1} surface [35]. Since Pt catalysts with higher Pt dispersion, *i.e.* smaller Pt particles, contain more stepped {2 1 1} surfaces, they are expected to exhibit higher activity for H_2-SCR reaction. Recently, a correlation of

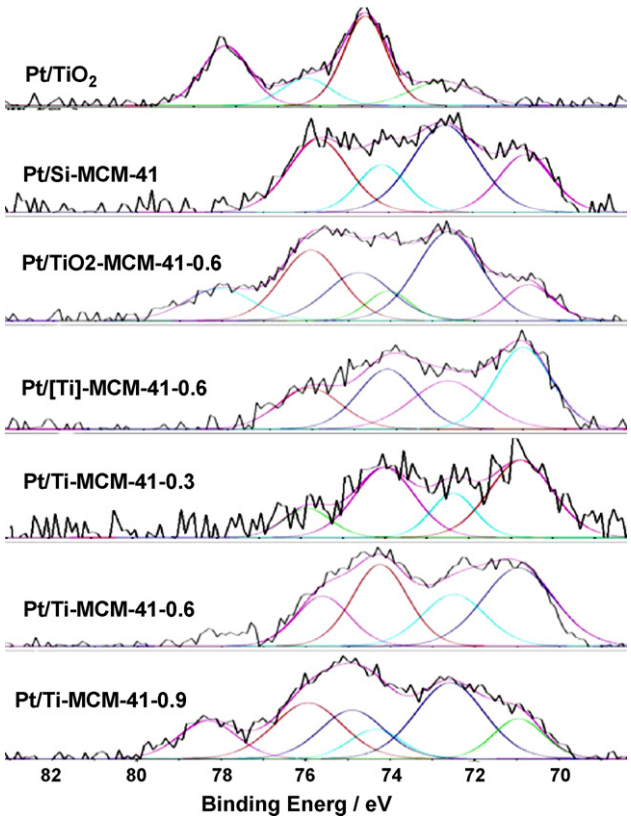

Fig. 7. XPS of Pt 4f region of different Pt catalysts.

dispersion on the specific rate of H_2-SCR on Pt/MgO–CeO_2 is reported and the specific reaction rate drops dramatically by increasing the Pt particle size from 1.3 to 4.0 nm [11].

In summary, the promotion effect of Ti species in Pt catalysts supported on Ti-containing MCM-41 comes from the formation of Pt-Ti interaction, which is reflected as the changes in Pt valence distribution and Pt dispersion. In this study, Pt/Ti–MCM-41-0.6 with highest Pt^0 proportion and highest Pt dispersion exhibits the best activity for H_2-SCR reaction.

3.4. The promotion effect of Ti species in Pt/Ti–SBA-15 and Pt/Ti–MCM-48

As discussed in the above section, highly dispersed anatase TiO_2 nanoparticles embedded in mesoporous structure of MCM-41 shows great promotion effect on NO selective reduction by hydrogen over Pt/MCM41 and this kind of promotion effect is supposed to exist for Pt catalysts supported on other mesoporous

Table 3
Dispersion[a] and valence distribution[b] of Pt in different Pt catalysts.

Catalyst	Existence status of Pt species			Pt dispersion
	Pt^0	$Pt^{II}O$	$Pt^{IV}O_2$	
Pt/TiO_2	–	29.6%	70.4%	43.1%
Pt/Si–MCM-41	35.2%	64.8%	–	33.4%
Pt/[Ti]–MCM-41-0.6	53.1%	46.9%	–	40.7%
Pt/TiO_2–MCM-41-0.6	13.7%	61.9%	24.4%	61.9%
Pt/Ti–MCM-41-0.3	63.1%	36.9%	–	57.7%
Pt/Ti–MCM-41-0.6	64.7%	35.3%	–	74.3%
Pt/Ti–MCM-41-0.9	22.6%	57.3%	20.1%	51.9%

[a] Determined by H_2 chemisorption.
[b] Determined by XP spectra.

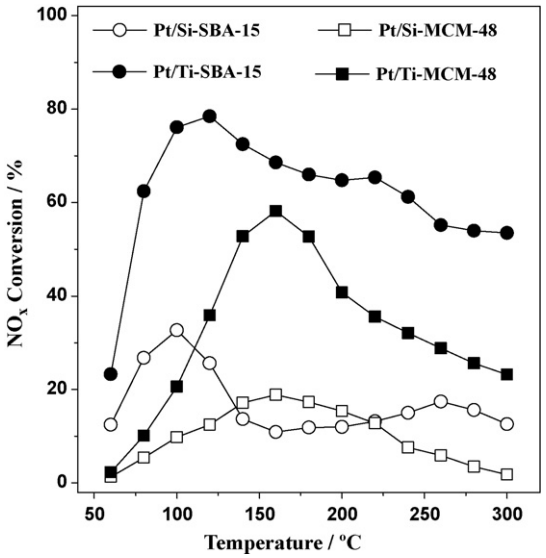

Fig. 8. NO selective reduction by hydrogen on Pt/Si–SBA-15, Pt/Ti–SBA-15 (Ti/Si = 0.6), Pt/Si–MCM-48 and Pt/Ti–MCM-48 (Ti/Si = 0.6). *Reaction conditions*: NO = 1000 ppm, H_2 = 5000 ppm, O_2 = 6.7%, He balance, GHSV = 80,000 h^{-1}.

materials. As seen in Fig. 8, the activities of Pt/Si–SBA-15 and Pt/Si–MCM-48 are greatly promoted with the introduction of Ti species by wet impregnation with Ti/Si of 0.6. The maximal NO_x conversions increase from *ca.* 33% to *ca.* 78% and from *ca.* 19% to *ca.* 58% on Pt/SBA-15 and Pt/MCM-48, respectively. Further characterization results (not shown here) indicate that the Ti species also exist in the form of isolated Ti atoms and highly dispersed anatase nanoparticles embedded in the mesoporous structure (SBA-15 or MCM-48). The promotion effect is attributed to the formation

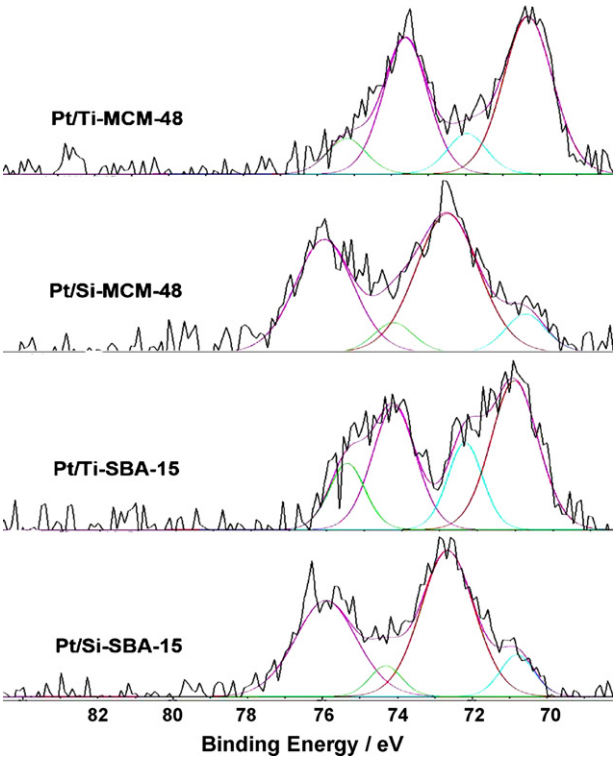

Fig. 9. XPS of Pt 4f region of Pt/Si–SBA-15, Pt/Ti–SBA-15 (Ti/Si = 0.6), Pt/Si–MCM-48 and Pt/Ti–MCM-48 (Ti/Si = 0.6).

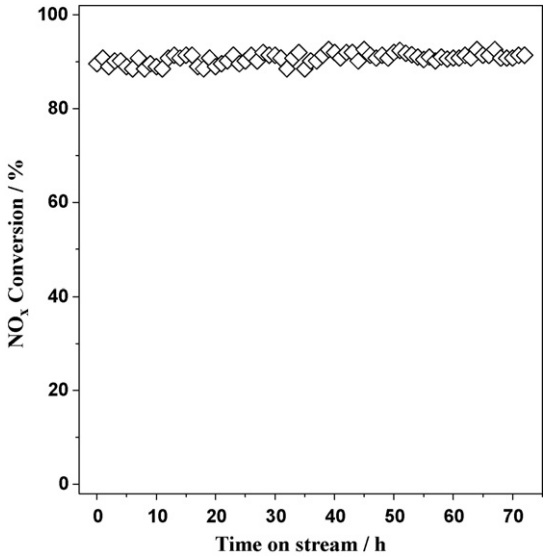

Fig. 10. Time-on-stream behavior of Pt/Ti–MCM-41-0.6 for H_2-SCR reaction at 140 °C. *Reaction conditions*: NO = 1000 ppm, H_2 = 5000 ppm, O_2 = 6.7%, He balance, GHSV = 80,000 h^{-1}.

Pt–Ti interaction and subsequent change in Pt existence status as well as Pt dispersion. As seen in Fig. 9, Pt species exist mainly in the form of oxides in Pt/Si–MCM-48 and Pt/Si–SBA-15. While after the introduction of Ti species by wet impregnation, a large proportion of Pt oxides are reduced to metallic Pt^0 by the electrons donated from Ti species to Pt species. Meanwhile, the Pt dispersion increases from 30.2% (Pt/Si–SBA-15) to 68.2% (Pt/Ti–SBA-15) and from 29.3% (Pt/Si–MCM-48) to 61.5% (Pt/Ti–MCM-48), respectively. The results are in good accordance with those observed on Pt/Ti–MCM-41 and adequately demonstrate the promotion effect of Ti species on Pt/meseporous silica for H_2-SCR.

3.5. Durability and anti-poisonous properties of Pt/Ti–MCM-41

The durability and anti-poisonous properties of catalysts are very important for potential application of H_2-SCR technique. Recently, outstanding durability and anti-poisonous properties of Pt/MgO–CeO_2 catalyst has been achieved in H_2-SCR process under simulated conditions of industrial exhaust [36]. In this work, Pt/Ti–MCM-41 is regarded as promising catalyst for H_2-SCR due to its outstanding activity and N_2 selectivity in the reaction. Remarkably, Pt/Ti–MCM-41 also demonstrates high durability in H_2-SCR reaction. As shown in Fig. 10, there is no catalytic activity loss for 72 h at 140 °C and NO_x conversion is kept at *ca.* 90%. Actually, no obvious activity loss can be observed after discontinuous reaction for over 20 days in our experiments. The high durability of Pt/Ti–MCM-41 is probably related to the stable Pt active sites in catalyst. As discussed in above section, the active Pt^0 may be greatly stabilized by interaction with Ti species and MCM-41 mesoporous structure. XPS analysis (not shown here) reveals that Pt^0 is not oxidized to $Pt^{II}O$ or $Pt^{IV}O_2$ after H_2-SCR reaction at 140 °C for over 70 h. Since the existence of water is unavoidable in the exhaust [36,37], a preliminary study on the effect of water on the H_2-SCR activity is carried out with Pt/Ti–MCM-41 catalyst. Typically, the addition of 2.5% H_2O produces a barely detectable negative effect on NO_x conversion, *i.e.* NO_x conversion at 140 °C decrease within 5%, and the NO_x conversion (at 140 °C, with 2.5% H_2O) is quite stable for *ca.* 50 h. Pt/Ti–MCM-41 seems to be good catalyst even in the presence of 2.5% H_2O. However, it is far not enough to mention the industrial application of this catalyst only based on the results presented and further work is in progress.

Since under practical circumstances there are some SO_2 and CO in the stream, it is necessary to clarify their effects on H_2-SCR over Pt/Ti–MCM-41. First of all, we investigate the effect of co-existing SO_2 in the reaction gas stream on the NO_x conversion at temperature of 140 °C. As seen in Fig. 11, the presence of 20 ppm SO_2 does not show obvious negative effect on NO_x conversion over Pt/Ti–MCM-41. However, increasing the concentration of SO_2 to 50 ppm causes serious deactivation and NO_x conversion dramatically decreases from *ca.* 90% to *ca.* 30% after 5 h. With the removal of SO_2 from feed stream, the NO_x conversion gradually recovers to *ca.* 87%. The negative effect of SO_2 on Pt catalysts is presumably due to the formation of sulfur oxides on support materials other than on Pt sites [36]. Since Ti–MCM-41 is the type of material with weak interaction with SO_2, Pt/Ti–MCM-41 exhibits good SO_2 tolerance during H_2-SCR. Pt/Ti–MCM-41 is tolerant to SO_2 at low concentration (~20 ppm) and the deactivation by SO_2 at higher concentration (~50 ppm) is reversible to a great extent. The existence of CO also shows negative effect on NO_x conversion over Pt/Ti–MCM-41, as displayed in Fig. 11. More serious negative effect is observed at higher concentration of CO in the range of 100–1000 ppm. Fortunately, the deactivation by CO is also reversible and the NO_x conversion is easily recovered after removing inlet CO. The existence of CO always shows negative effect on NO reduction, due to the strong chemisorption of CO on Pt sites [38,39]. While in our reaction system, the chemisorption of CO on Pt sites is reversible and the desorption of CO may be promoted by the H_2 in the stream, as suggested by Costa et al. [36].

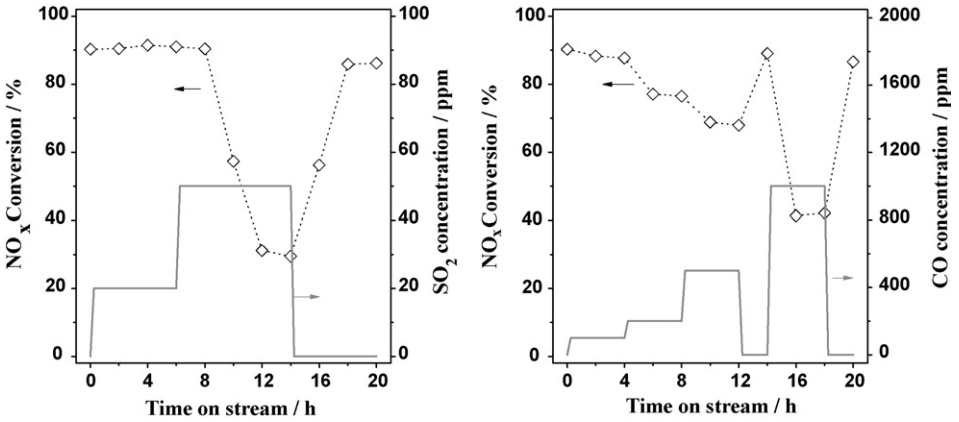

Fig. 11. Effect of co-existing CO or SO_2 in the feed on NO selective reduction over Pt/Ti–MCM-41-0.6 at 140 °C. *Reaction conditions*: NO = 1000 ppm, H_2 = 5000 ppm, CO = 0–1000 ppm, SO_2 = 0–50 ppm, O_2 = 6.7%, He balance, GHSV = 80,000 h^{-1}.

4. Conclusion

In this study, Pt catalysts supported on Si–MCM-41 and Ti-containing MCM-41 are investigated for NO selective reduction by hydrogen in excess oxygen. Among all catalysts, Pt/Ti–MCM-41 with Ti/Si ratio of 0.6 exhibits the best activity and a maximal NO_x conversion of *ca.* 89% can be achieved at 140 °C with N_2 selectivity of *ca.* 79%.

Characterization results reveal that different Ti species, *e.g.* isolated Ti atoms, highly dispersed anatase nanoparticles and bulk anatase TiO_2, are introduced to MCM-41 by different methods with the mesoporous structure well preserved. The introduced Ti species may interact with active Pt species, resulting in the changes in Pt existence status and Pt dispersion. In such a manner, different Ti speices may show different effects on Pt catalysts for H_2-SCR and the best promotion effect is obtained on highly dispersed anatase nanoparticles embedded in the mesoporous structure of MCM-41. Notably, the promotion effect of such Ti species is not limited to Pt/Ti–MCM-41 catalyst for H_2-SCR and similar promotion effect is also observed on Pt catalysts supported on other Ti-containing mesoporous materials, *e.g.* SBA-15 and MCM-48.

Acknowledgements

This work was financially supported National Natural Science Foundation of China (20973094, 20703057) and National Basic Research Program of China (2009CB623502). The support from International S&T Cooperation Program of China (ISCP) (2007DFA90720) is greatly appreciated.

References

[1] J.N. Armor, Environmental Catalysis, American Chemical Society, Washington, DC, 1994.
[2] P. Forzatti, L. Lietti, E. Tronconi, in: I.T. Horvath (Ed.), Nitrogen Oxides Removal – E (Industrial), Wiley, New York, 2002.
[3] R. Burch, P.J. Millington, A.P. Walker, Appl. Catal. B 4 (1994) 65–94.
[4] R. Burch, M.D. Coleman, Appl. Catal. B 23 (1999) 115–121.
[5] C.N. Costa, V.N. Stathopoulos, V.C. Belessi, A.M. Efstathiou, J. Catal. 197 (2001) 350–364.
[6] M. Machida, S. Ikeda, D. Kurogi, T. Kijima, Appl. Catal. B 35 (2001) 107–116.
[7] M. Machida, S. Ikeda, J. Catal. 227 (2004) 53–59.
[8] S. Hamada, K. Ikeue, M. Machida, Appl. Catal. B 71 (2006) 1–6.
[9] J. Shibata, M. Hashmoto, K. Shimizu, H. Yoshida, T. Hattori, A. Satsuma, J. Phys. Chem. B 108 (2004) 18327–18335.
[10] M. Machida, T. Watanabe, Appl. Catal. B 52 (2004) 281–286.
[11] C.N. Costa, A.M. Efstathiou, Appl. Catal. B 72 (2007) 240–252.
[12] N. Macleod, R.M. Lambert, Catal. Commun. 3 (2002) 61–65.
[13] M. Engelmann-Pirez, P. Granger, G. Leclercq, Catal. Today 107–108 (2005) 315–322.
[14] G. Qi, R.T. Yang, F.C. Rinaldi, J. Catal. 237 (2006) 381–392.
[15] L.D. Li, F.X. Zhang, N.J. Guan, E. Schreier, M. Richter, Catal. Commun. 9 (2008) 1827–1832.
[16] C.N. Costa, A.M. Efstathiou, J. Phys. Chem. B 108 (2004) 2620–2630.
[17] C.N. Costa, A.M. Efstathiou, J. Phys. Chem. C 111 (2007) 3010–3020.
[18] P.G. Savva, A.M. Efstathiou, J. Catal. 257 (2008) 324–333.
[19] R.Q. Long, R.T. Yang, Catal. Lett. 52 (1998) 91–96.
[20] S.C. Shen, S. Kawi, Appl. Catal. B 45 (2003) 63–76.
[21] J.Y. Jeon, H.Y. Kim, S.I. Woo, Appl. Catal. B 44 (2003) 311–323.
[22] P. Wu, Y.X. Liu, F.X. Zhang, L.D. Li, Y.L. Yang, N.J. Guan, Acta Phys. Chim. Sinca 24 (2008) 369–374.
[23] C.T. Kresge, M.E. Leonowicz, W.J. Roth, J.C. Vartuli, J.S. Beck, Nature 359 (1992) 710–712.
[24] W. Su, J. Zhang, Z. Feng, T. Chen, P. Ying, C. Li, J. Phys. Chem. C 112 (2008) 7710–7716.
[25] S. Klein, B.M. Weckhuysen, J.A. Martens, W.F. Majer, P.A. Jacobs, J. Catal. 163 (1996) 489–491.
[26] J. Klaas, G. Schulz-Ekloff, N.I. Jaeger, J. Phys. Chem. B 101 (1997) 1305–1311.
[27] L. Marchese, T. Maschmeyer, E. Gianotti, S. Coluccia, J.M. Thomas, J. Phys. Chem. B 101 (1997) 8836–8838.
[28] W. Zhang, M. Froba, J. Wang, P.T. Tanev, J. Wong, T.J. Pinnavaia, J. Am. Chem. Soc. 118 (1996) 9164–9171.
[29] H. Iida, A. Igarashi, Appl. Catal. A 298 (2006) 152–160.
[30] W.Y. Teoh, L. Mädler, R. Amal, J. Catal. 251 (2007) 271–280.
[31] C.D. Wagner, W.M. Riggs, L.E. Davis, J.F. Moulder, G.E. Muilenberg, Handbook of X-ray Photoelectron Spectroscopy: A Reference Book of Standard Data for Use in X-ray Photoelectron Spectroscopy, Perkin-Elmer, Eden-Prairie, MN, 1979.
[32] S.H. Chien, B.N. Shelimov, D.E. Resasco, E.H. Lee, G.L. Haller, J. Catal. 77 (1982) 301–303.
[33] S.C. Shen, S. Kawi, J. Catal. 213 (2003) 241–250.
[34] J.Y. Jeon, H.Y. Kim, S.I. Woo, Appl. Catal. B 44 (2003) 301–310.
[35] Z.P. Liu, S.J. Jenkins, D.A. King, J. Am. Chem. Soc. 125 (2003) 14660–14661.
[36] C.N. Costa, P.G. Savva, J.L.G. Fierro, A.M. Efstathiou, Appl. Catal. B 75 (2007) 147–156.
[37] G.C. Mondragon Rodriguez, B. Saruhan, Appl. Catal. B: Environ. (2009), doi:10.1016/j.apcatb.2009.10.004.
[38] T.P. Kobylinski, B.W. Taylor, J. Catal. 33 (1974) 376–384.
[39] K. Yokota, M. Fukui, T. Tanaka, Appl. Surf. Sci. 121/122 (1997) 273–277.